JACS
JOURNAL OF THE AMERICAN CHEMICAL SOCIETY
Cite This: J. Am. Chem. Soc. 2018, 140, 8958−8964
Article
pubs.acs.org/JACS

Impact of Disordered Guest−Framework Interactions on the Crystallography of Metal−Organic Frameworks

Seungkyu Lee,[†] Hans-Beat Bürgi,[‡,§] Sultan A. Alshmimri,[⊥] and Omar M. Yaghi*[,†,⊥]

[†]Department of Chemistry, University of California—Berkeley; Materials Sciences Division, Lawrence Berkeley National Laboratory; Kavli Energy NanoSciences Institute at Berkeley; and Berkeley Global Science Institute, Berkeley, California 94720, United States

[‡]Department of Chemistry and Biochemistry, University of Bern, Freiestrasse 3, 3012 Bern, Switzerland

[§]Department of Chemistry, University of Zurich, Winterthurerstrasse, 190, 8057 Zurich, Switzerland

[⊥]King Abdulaziz City for Science and Technology, Riyadh 11442, Saudi Arabia

Supporting Information

ABSTRACT: It is a general and common practice to carry out single-crystal X-ray diffraction experiments at cryogenic temperatures in order to obtain high-resolution data. In this report, we show that this practice is not always applicable to metal−organic frameworks (MOFs), especially when these structures are highly porous. Specifically, two new MOFs are reported here, MOF-1004 and MOF-1005, for which the collection of the diffraction data at lower temperature (100 K) did not give data of sufficient quality to allow structure solution. However, collection of data at higher temperature (290 K) gave atomic-resolution data for MOF-1004 and MOF-1005, allowing for structure solution. We find that this inverse behavior, contrary to normal practice, is also true for some well-established MOFs (MOF-177 and UiO-67). Close examination of the X-ray diffraction data obtained for all four of these MOFs at various temperatures led us to conclude that disordered guest−framework interactions play a profound role in introducing disorder at low temperature, and the diminishing strength of these interactions at high temperatures reduces the disorder and gives high-resolution diffraction data. We believe our finding here is more widely applicable to other highly porous MOFs and crystals containing highly disordered molecules.

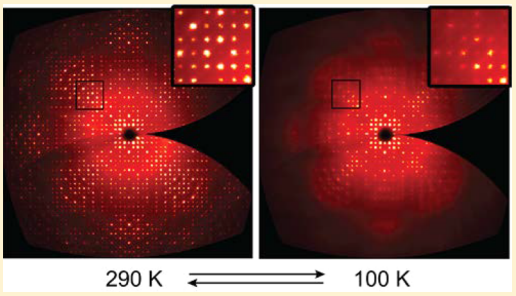

INTRODUCTION

In X-ray crystallography, structural (static) and thermal disorder (vibrational) are obstacles to obtaining high-resolution diffraction data and accurate crystal structures. It is a general practice to acquire such data at cryogenic temperatures where thermal disorder is reduced, thereby allowing the diffraction of X-rays to higher angles.[1,2] Indeed, this practice is routinely applied to crystals of small and large molecules as well as extended structures such as the members of the extensive class of metal−organic frameworks (MOFs).[3] In this report, we show that, for two new MOF crystals (MOF-1004 and MOF-1005), the diffraction data collected at low temperature (100 K) were of low quality, impeding structure determination. However, contrary to the common experience, we have obtained improved data sets to atomic resolution at higher temperature (290 K), allowing easier structure solution and refinement. Given this unusual observation, we also examined crystals of two archetypical MOFs (MOF-177 and UiO-67) and found that they exhibit the same trend.[4,5] Our studies of the diffraction behavior of the four MOFs at various temperatures show that the evolution of total disorder in these crystals is inverse to that generally observed in crystal structure determination. This observation suggests that the disordered guest molecules impinge on the frameworks and cause disorder in the flexible backbone of the MOFs. This effect is larger at low temperature and smaller at higher temperature, and accordingly impacts the quality of diffraction data. This scenario is supported by collecting data on corresponding evacuated crystals of the MOFs, where the inverse behavior was not observed. The effect of the disordered interactions was further investigated with a mechanically robust MOF, UiO-66.[5,6] The internal structure of UiO-66 filled with guests does not show the inverse behavior but is still affected by the disordered interactions, thus losing X-ray scattering power at the resolution limit by multiple folds compared to the interaction-free evacuated crystal. Although there are reports concerned with guest-induced crystal structure changes (e.g., breathing effects, unusual thermal expansions, and symmetry changes) under various conditions, the disordered guest−framework interactions have not been the main focus of those studies.[7−14] Our findings are expected to impact how we collect data on crystals of MOFs and other reticular

Received: May 19, 2018
Published: June 25, 2018

DOI: 10.1021/jacs.8b05271
J. Am. Chem. Soc. 2018, 140, 8958−8964

frameworks (covalent organic frameworks), including highly solvated crystals containing disordered solvent.

EXPERIMENTAL SECTION

X-ray Data Collection at a Synchrotron. The synthesis and characterization of the MOFs in this work are described in the Supporting Information (SI, Figures S1−S5 and Tables S1 and S2). The pore of the as-synthesized MOF-1004 was evacuated following a general activation procedure using anhydrous acetone for the solvent exchange and a supercritical CO_2 drier to minimize pore collapse during solvent removal. The evacuated MOF-1004 was soaked in *N*,*N*′-dimethylformamide (DMF) for 3 days to charge the pores with the guest molecules. A single crystal of MOF-1004 (∼100 μm) with DMF was mounted on a goniometer equipped with a liquid nitrogen cryostream whose temperature was preset to 290 K (synchrotron beamline 11.3.1 at the Advanced Light Source). Full sets of data were collected in ∼4 min with wavelength 1.1271 Å (11 keV) starting at 290 K. Between data collections, the shutter was kept closed to minimize beam damage, and the temperature was reduced by 30 K at a rate of 0.1 K s^{-1}. The same experimental conditions were applied for data collections during temperature increase. These experiments were also applied to MOF-1005 data collection, but the initial data collection temperature was set as 260 K.

X-ray Data Collection with an In-House Diffractometer. The experiments for MOF-177, UiO-66, and UiO-67 were carried out with an in-house instrument (Bruker D8 Venture system equipped with Photon II detector) that requires much longer data collection times compared to the synchrotron experiment. Since pore collapse due to guest evaporation has frequently been observed at 290 K in such experiments, the upper temperature was set to 260 K to retain DMF molecules in the pores. The temperature was changed at a rate of 0.1 K s^{-1} between data collections.

RESULTS AND DISCUSSION

Specifically, we studied crystals of two new MOFs, MOF-1004, $Zr_6(\mu_3\text{-}O)_4(\mu_3\text{-}OH)_4(BTE)_4$ (BTE = 4,4′,4″-[benzene-1,3,5-triyltris(ethyne-2,1-diyl)]tribenzoate), and MOF-1005, $Zr_6(\mu_3\text{-}O)_4(\mu_3\text{-}OH)_4(OH)_4(H_2O)_4(BBC)_{8/3}$ (BBC = 4,4′,4″-[benzene-1,3,5-triyltris(benzene-4,1-diyl)]tribenzoate), the well-known MOF-177, $Zn_4O(BTB)_2$ (BTB = 1,3,5-benzenetribenzoate), and UiO-67, $Zr_6(\mu_3\text{-}O)_4(\mu_3\text{-}OH)_4(BPDC)_6$ (BPDC = 1,4-biphenyldicarboxylate). All these MOFs show increased disorder of the framework at reduced temperatures. We studied this unexpected effect on the frameworks by analyzing the temperature dependence of single-crystal X-ray diffraction (SXRD) patterns, their resolution, Wilson plots,[15] changes in the framework structure, atomic displacement parameters (ADPs),[16] and electron difference density maps attributed to the guest molecules. UiO-67 was chosen to gain additional insight into the phenomenon by examining the dependency of the inverse behavior on the concentration of missing linker defects.[6] Finally, although UiO-66, $Zr_6(\mu_3\text{-}O)_4(\mu_3\text{-}OH)_4(BDC)_6$ (BDC = 1,4-benzenedicarboxylate), did not exhibit the inverse behavior, which is attributable to its high mechanical stability, it was further investigated to show that the disordered guests in the pore still cause a noticeable disorder on the framework, thus reducing X-ray scattering power at high angles. Partial organization of the guests was achieved by a temperature swing procedure, and the effect of the organization on the structure and diffraction intensity of UiO-66 was studied. Subsequently, the guests were removed by heating the crystal, and a multiple folds higher $\langle I/\sigma \rangle$ value was obtained around the resolution limit compared to the value of the crystal filled with guests.

Structures of MOF-1004 and MOF-1005. The framework of MOF-1004 is composed of 12-coordinated secondary building units (SBUs), $Zr_6(\mu_3\text{-}O)_4(\mu_3\text{-}OH)_4(\text{-}COO)_{12}$, and tritopic BTE linkers forming this new MOF with a new net, now registered as **sky** in the Reticular Chemistry Structure Resource (Figure 1a).[17] The structure with space group $Pm\bar{3}n$ and a unit cell parameter of 41.367(4) Å accommodates a high-symmetry mesopore in the center of the unit cell with a diameter of 33.38 Å (shortest non-hydrogen interatomic distance across the center of the pore, point group: *m*-3). The pore has eight window openings, 18.35 Å, along the 3-fold axes. Additionally, there are three non-intersecting channels parallel to the unit cell axes. MOF-1005 is isoreticular to a known MOF, BUT-12.[18] MOF-1005 crystallizes in the space

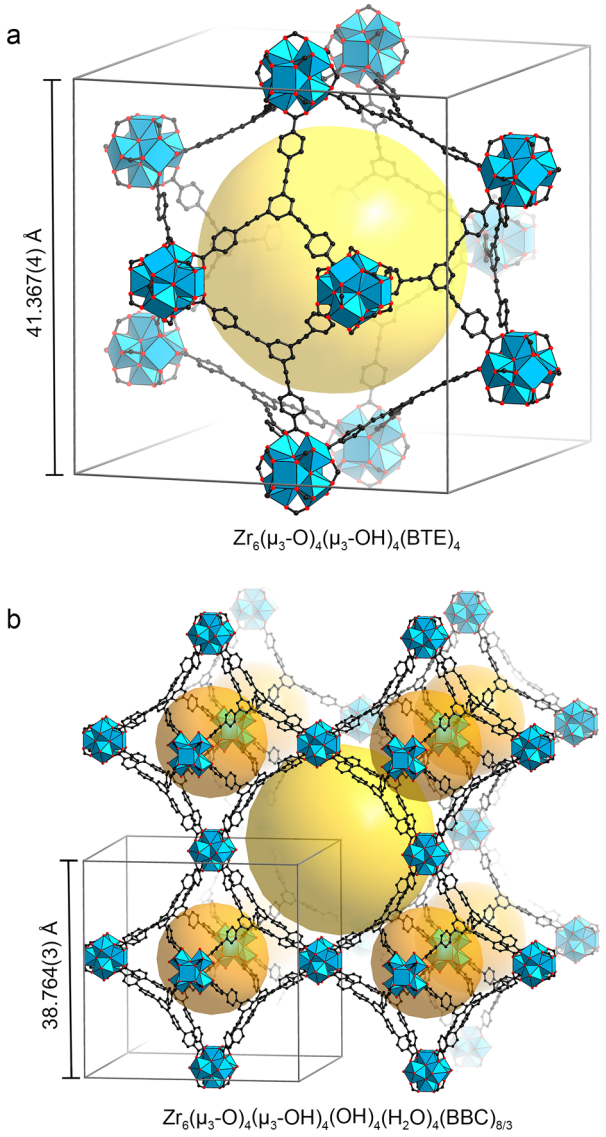

Figure 1. Refined structures of MOF-1004 and MOF-1005 from single-crystal X-ray diffraction data. The structures are shown in ball-and-stick models for carbon and oxygen and blue polyhedra for Zr. The pore of MOF-1004 is indicated with a yellow ball located on the center of the unit cell (a). The structure of MOF-1005 has two kinds of pores that are located at the center and corners of the unit cell, indicated by orange and yellow balls, respectively (b). Color code: black, C; red, O.

DOI: 10.1021/jacs.8b05271
J. Am. Chem. Soc. 2018, 140, 8958−8964

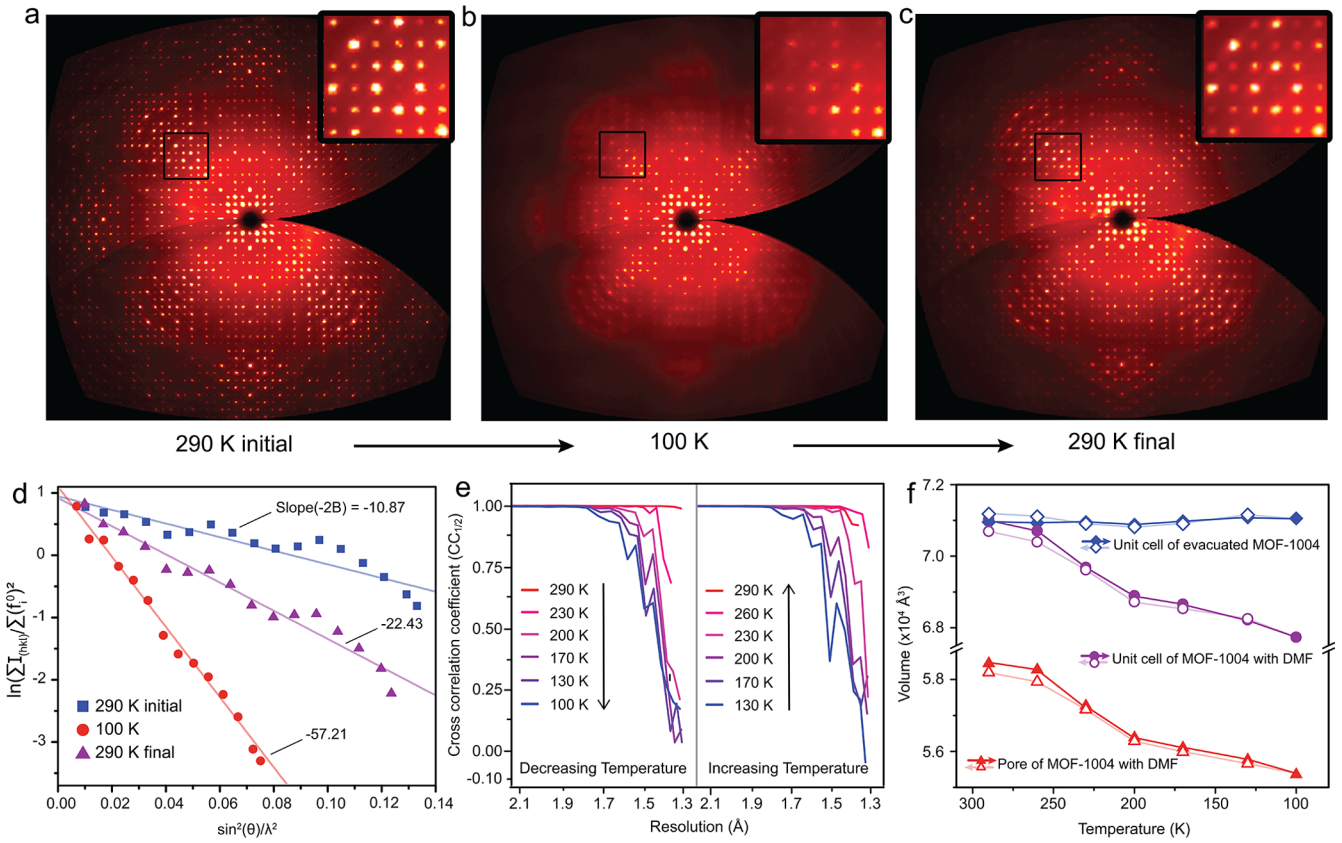

Figure 2. Temperature-dependent diffraction analysis of MOF-1004 charged with DMF. (a–c) Reconstruction images of (*hk*0) of the data collected at 290, 100, and 290 K, respectively. (d) Wilson plots of the corresponding data. (e) Cross correlation coefficients of the data sets collected at various temperatures. (f) Unit cell volume changes of the MOF with guests and the evacuated MOF, and volume changes of the solvent-accessible area of the crystal with the guests.

group $Pm\bar{3}m$ with unit cell parameter 38.764(3) Å and features two different types of pore with diameters of 41.56 and 25.82 Å, which are located at the origin and center of the unit cell, respectively (Figure 1b). The large pore openings and underlying self-dual nature of the framework allow interpenetration. Structure refinement of the SXRD data indicates the second framework with ~20% occupancy.[19]

Reciprocal Space Analysis. For guest-filled MOF-1004, the images of the Bragg reflections in the (*hk*0) layer were reconstructed for 290 down to 100 K, and back to 290 K (Figure 2a–c). They show that upon cooling to 100 K, the weaker reflections, especially those at high diffraction angles are no longer visible, but are clearly visible when the sample is heated back to 290 K. The changes in resolution were characterized quantitatively for the full data set and found to be 1.35, 2.07, and 1.53 Å at 290, 100, and 290 K, respectively, for $\langle I/\sigma \rangle$ = 9. The initial resolution of 1.35 Å was not recovered entirely in the final data, possibly due to radiation damage, which is also observed in the evacuated MOF-1004 (Figures S6 and S7). Also slight increase of the mosaicity (slight misorientation of the blocks in the crystal specimen) was observed over the course of the data collections, where the values 0.57, 0.59, and 0.59° are found for 290, 100, and 290 K, respectively (Table 1). Wilson plots show the decay of the average scattering intensity in a log scale with increasing diffraction angle. The slope of the corresponding linear fit is $-2B$, where B is proportional to the average atomic mean square displacement for all atoms in the unit cell (Figure 2d). The data analysis indicates that B increases, upon cooling, from 5.4 to 28.6 Å^2 and decreases back to 11.2 Å^2 when warming, where the smaller B corresponds to more well-defined atomic positions in the structure. The cross correlation coefficient $CC_{1/2}$ between random half data sets is used to estimate the resolution limit of a diffraction data set.[20] Irrespective of the specific resolution cutoff criterion chosen, the room-temperature data showed better correlation and thus better data at high diffraction angles than the low-temperature data (Figure 2e). An evacuated MOF-1004 was investigated as a control experiment where this disorder trend was not observed (Figures S6 and S7). The resolutions at $\langle I/\sigma \rangle$ = 9 are 1.32, 1.44, and 1.44 Å at 290, 100, and 290 K, respectively, and the corresponding B values are 7.2, 7.3, and 9.8 Å^2 (Table S3). Wilson plots and cross correlation coefficient $CC_{1/2}$ data of the evacuated MOF are shown in Figure S7.

Direct Space Analysis. The volume changes of the unit cell of the MOF-1004 crystals are plotted along with that of its evacuated form (Figure 2f). About 5.7% decrease in cell volume was observed at 100 K. The changes of the pore volume follow the same trend, which suggests that the contraction is mainly due to the presence of guests. In contrast, the volume of the evacuated MOF remains essentially constant throughout the temperature range. The projection images, along [100], of the refined structures of the evacuated and DMF filled MOF collected at 290 and 100 K are shown in Figure 3a–c. Upon loading the crystal with DMF, the central phenyl ring of the nominally planar BTE linker moves toward the center of the pore by ~0.6 Å. After cooling, this distance increases to ~1.2 Å, further reducing the volume of the pore.

DOI: 10.1021/jacs.8b05271
J. Am. Chem. Soc. 2018, 140, 8958–8964

Table 1. Temperature-Dependent Structure Parameters and Data Quality of Various MOFs

MOFs with DMF	temp (K)	Wilson B (Å^2)	metal ADPs (Å^2)	volume (Å^3) void	volume (Å^3) unit cell	resolution (Å) at $\langle I/\sigma \rangle = 9$	mosaicity (deg)	space group
MOF-1004	290 (initial)	5.435	0.0862(45)	58412	70788(14)	1.35	0.57	$Pm\bar{3}n$
	100	28.61	0.36225(417)	54326	66731(18)	2.07	0.59	
	290 (final)	11.26	0.16888(86)	58083	70489(9)	1.53	0.59	
MOF-1005	260	11.31	0.1539(15)[c]	49780	58246(7)	1.48	0.67	$Pm\bar{3}m$
	100	–[b]	–	–	55882(189)	2.96	0.67	
	260	10.99	0.2081(47)	50344	58485(11)	2.13	0.67	
MOF-177	260	6.359	0.097(20)	26735	35469(3)	1.72	0.70	$P\bar{3}1c$
	100	–	–	–	33741(5)	3.29	0.71	
	260	5.918	0.129(47)	27337	35468(6)	1.95	0.73	
UiO-66 (17.2(11)% defect)[a]	260	0.4834	0.00915(18)	4636[d]	8973.5(12)	0.77 (11.08)[e]	0.67	$Fm\bar{3}m$
	100	0.2608	0.00579(24)	4584	8930.3(10)	0.77 (20.78)	0.66	
	260	0.4720	0.00858(24)	4614	8957.1(10)	0.77 (15.37)	0.65	
UiO-67 (4.7(7)% defect)	260	0.6859	0.00890(35)	13146	19322(2)	0.84	0.64	$Fm\bar{3}m$
	100	0.3189	0.00526(33)	13009	19162.8(17)	0.80	0.64	
	260	0.5146	0.00832(30)	13114	19249(2)	0.82	0.63	
UiO-67 (12.5(7)% defect)	260	0.4476	0.01058(17)	13130	19333.9(10)	0.81	0.71	$Fm\bar{3}m$
	100	0.3338	0.00960(20)	12972	19137.2(7)	0.81	0.71	
	260	0.3109	0.00916(18)	13125	19337.3(10)	0.81	0.72	
UiO-67 (21.2(4)% defect)	260	0.6993	0.01420(12)	13168	19339.9(8)	0.80 (19.58)	0.71	$Fm\bar{3}m$
	100	3.334	0.0708(14)	12833	19000.0(17)	1.34	0.77	
	260	1.018	0.0197(26)	13185	19304.9(8)	0.81	0.75	

[a]Defect values are averaged from the structures that were collected at the three different temperatures. [b]Data quality is insufficient to refine the structure. [c]When there are multiple types of metal in a structure, an averaged value is reported. [d]Void volumes are calculated assuming ideal crystals without defects. [e]In the cases that the highest resolution of a data set has a higher $\langle I/\sigma \rangle$ value than 9, the $\langle I/\sigma \rangle$ value at the resolution is reported in parenthesis next to the resolution.

This means DMF is occupying less space and interacts more strongly with the framework. More direct information on the pore content is accessible from the electron density distribution within the pore (see SI, Section S2.2, for technical details). The densities in the (111) plane passing through the center of the unit cell are compared in Figure 3d–f. They represent the averaged arrangements of the guests in the pores. We have been unable to model them convincingly as DMF molecules because they are heavily disordered. However, the highest densities are within ~4 Å of the framework atoms in this plane, i.e., within a reasonable distance between non-bonded atoms. The electron densities at 100 K appear more localized indicating that DMF guests are less mobile and more ordered, while the framework is now more disordered as indicated, for example, by the ADPs of the Zr atom, 0.086(5), 0.36(4), and 0.168(1) Å^2 at 290, 100, and 290 K, respectively (Table 1).

Based on these observations, we postulate the following: the guest-framework interactions are weaker at 290 K, so the displacement of the framework from the averaged position is smaller. In addition, relatively free movement of the guests can relieve the strain by virtue of their rearrangement. On the other hand, the guests at lower temperatures have stronger interactions with the framework and the contraction induces significant deviations from the averaged positions. Moreover, the strain is more difficult to be relieved because the movements of guests at lower temperatures are more restricted. Such deviations in the atomic positions of the framework across the single crystal are poorly correlated as the disordered guests can induce varying degrees of deviations in different unit cells across the crystal. As a result, the reduction of scattering power of the disordered framework is reduced and is reflected in weaker high angles diffraction data.

Disordered Interactions in Other MOFs. The increase of disorder induced by guests at low temperature was also observed in MOF-1005, MOF-177, and UiO-67 crystals. The results of the analysis of the collected data are summarized in Table 1. For UiO-67, three single crystals with missing linker percentages of 4.7, 12.5, and 21.2% were identified based on the structure refinements. A trend was observed in the three data sets that as the amount of the defects increases, the reduction of the structural disorder upon cooling is less pronounced. The crystal with 4.7% defects showed the largest decrease in Wilson B-factor and metal ADP values upon cooling among the three crystals. The crystal with 12.5% defects showed a marginal decrease of the values. For example, the Zr ADP value was reduced from 0.011 to 0.010 Å^2. The crystals with 21.2% defects showed the inverse behavior. A single crystal of UiO-66 with 17.2% defects exhibited a noticeable reduction of the structural disorder upon cooling (Zr ADP from 0.009 to 0.006 Å^2) in spite of its higher defect concentration compared to the data sets of UiO-67 with 12.5%

DOI: 10.1021/jacs.8b05271
J. Am. Chem. Soc. 2018, 140, 8958–8964

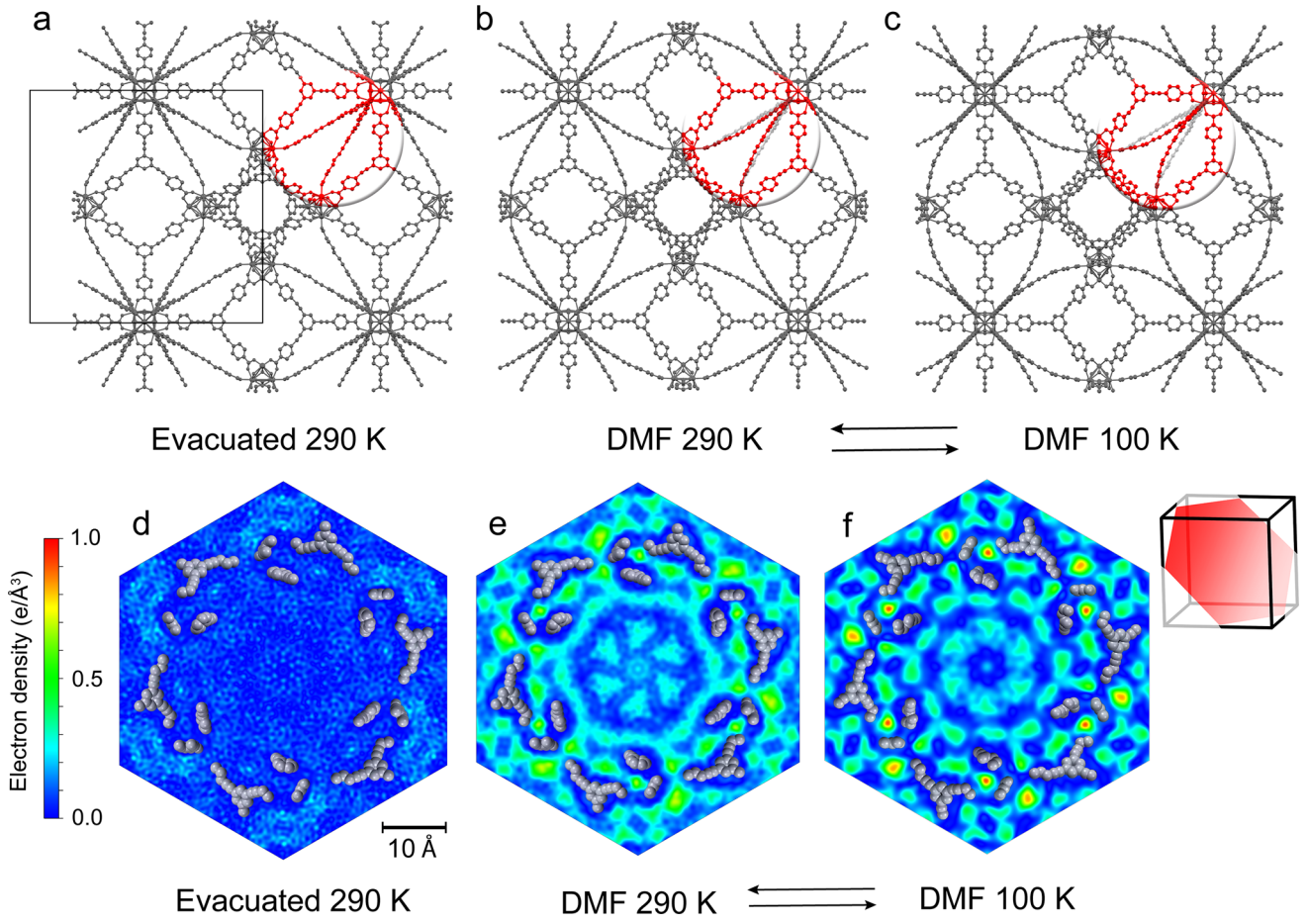

Figure 3. Temperature-dependent structure distortions of MOF-1004 and averaged electron densities of the guests in the pore. (a–c) Projection images along [100] of the refined structures of MOF-1004 with and without DMF, from the data collected at 290 and 100 K. Distortion of the linker is emphasized with red color in circles. (d–f) Fourier synthesized electron density maps of (111) planes of the evacuated MOF-1004 measured at 290 K, and the MOF with the guest molecules measured at 290 and 100 K, respectively. The gray space-filling models of the frameworks sliced by the plane are embedded.

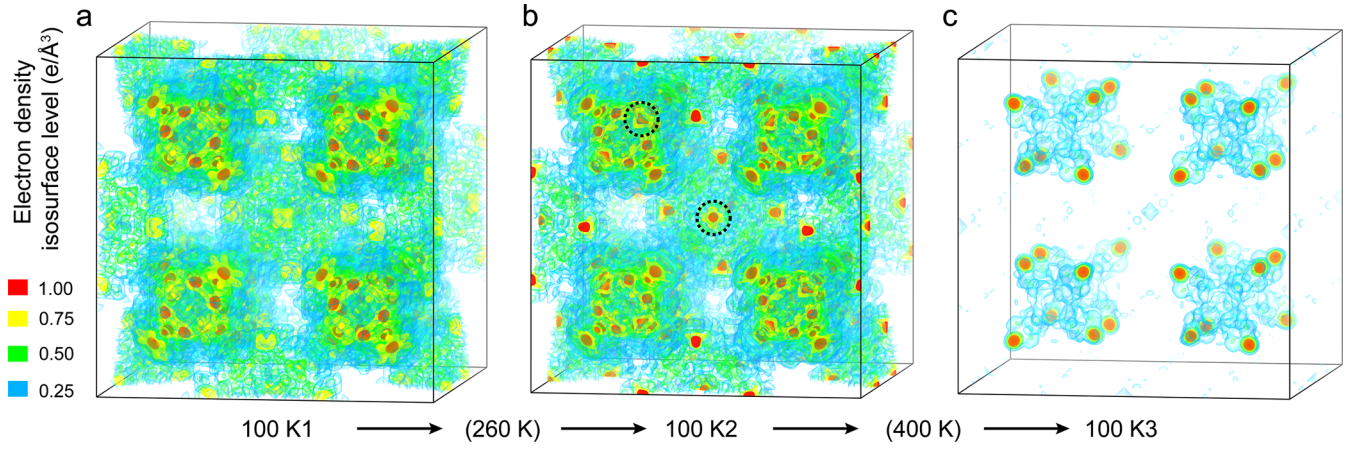

Figure 4. Fourier-synthesized electron density in the pores of UiO-66 through temperature swing. (a–c) The electron density maps of the guest molecules in the tetrahedral (1/4, 1/4, 1/4) and the octahedral (1/2, 1/2, 1/2) pores of the unit cell are Fourier synthesized, where the framework is masked out. The levels of the electron density are indicated by red, yellow, green, and blue isosurfaces. All three data are collected at 100 K, and the temperatures reached between the measurements are indicated in parentheses.

defect. Since we do not have control on picking up crystals with a certain defect concentration, it was impossible to study the effect of pore size on the disorder with the isoreticular UiO series having the same degree of defects. However, our experiments indicate that, in general, the disordered interactions are more pronounced in MOFs with higher porosity, such as MOF-1004, 1005, and 177, and the interactions are related to structural stability as shown with the three defective UiO-67 crystals. The (*hk*0) reconstruction images and the

DOI: 10.1021/jacs.8b05271
J. Am. Chem. Soc. 2018, 140, 8958–8964

parameters of the corresponding evacuated MOFs are shown in Figures S8−S15 and Table S3.

Disordered Interactions in Mechanically Robust UiO-66. We chose UiO-66 to study the organization of guest molecules by temperature swing and dependency of the diffraction intensity on the presence and absence of the guests. A single crystal of UiO-66 charged with DMF was mounted on the goniometer at the synchrotron where the temperature was preset to 100 K, and the data set 100 K1 was collected. The electron density map of the guests in the pores is shown in Figure 4a, where the framework is masked out. Electron densities are found in two different types of pore of tetrahedral and octahedral shapes, the centers of which are located at 1/4, 1/4, 1/4 and 1/2, 1/2, 1/2 of the unit cell, respectively. After the data collection, the temperature was increased to 260 K and cooled down to 100 K at a rate 0.1 $Ks^{-1}$to see if the arrangement of guest molecules is affected by the temperature swing. The electron density map obtained from data set 100 K2 is shown in Figure 4b. Although the two data sets were collected at the same temperature, more localized densities on the corners of the octahedral and tetrahedral pores were observed compared to data set 100 K1. The localized area is emphasized in circles embedded in Figure 4b. This result shows that the heavily disordered guests in the pores of the MOF become more ordered with the temperature swing. Even if there is doubt that the guests can be completely ordered by an optimized temperature swing, it might indeed be possible to improve the characterization of dangling functionalities or molecules bound to the backbone within the pores as in crystalline sponge and coordinative alignment methods.[21,22]

Subsequently, the temperature was increased to 400 K and kept for an hour to evaporate the guest molecules. The crystal was cooled down to 100 K again, and data set 100 K3 was collected. The density map shows that the guests are evaporated, and most of residual densities are observed in the tetrahedral pores (Figure 4c). The numbers of electrons found in the pores for 100 K1, K2, and K3 are 1459 (∼36 DMF), 1350 (∼34 DMF), and 384 (∼10 DMF), respectively (based on a theoretical calculation considering only the density (4 molecules/408.6 $Å^3$) of DMF in its crystalline form and the accessible pore volume (4636 $Å^3$), maximum ∼45 DMF molecules can fit in the pore).[23] The intensity statistics of the three data sets sorted by resolution are shown in Table S4. The statistics of data set 100 K2 presents a slight improvement of $\langle I/\sigma \rangle$ value compared to 100 K1 in a resolution range, 0.80 to 0.75 Å, attributable to the guests organization induced by the temperature swing. Data set 100 K3 has a substantially improved $\langle I/\sigma \rangle$ value about three folds higher than that of 100 K2. The values found for 100 K1, K2, and K3 are 5.7, 6.2, and 20.2, respectively. The Fourier transformation of the further spread out reflections of the evacuated MOF to higher resolution is reflected in the localized atomic positions of the internal structure (Figure S16). For example, the ADPs of the *ortho*-carbon on the phenyl ring, which is relatively far from the SBU and thus subject to the interactions with the guests, are 0.76, 0.73, and 0.34 $Å^2$ for the refined structures of 100 K1, K2, and K3, respectively. A similar experiment was carried out with a single crystal of UiO-66 with the in-house diffractometer, where the $\langle I/\sigma \rangle$ values for UiO-66 with DMF and the evacuated UiO-66 are found as 5.5 and 9.0, respectively, in a resolution range of 0.81 to 0.75 Å (Table S6). This result indicates that UiO-66, known for its high mechanical stability, is still affected by the disordered guest molecules and lose X-ray scattering power at high angles, although it does not exhibit the inverse behavior. These results led us to conclude that the disordered guests in the pores contribute to the intensities of Bragg reflections in two opposing ways: The enhanced X-ray scattering power from the averaged electron density of DMF and reduced vibration of the framework by DMF[24] increase the intensities of Bragg reflections, while their disordered nature distorts the framework thereby decreasing the intensities at high angles. In this study, we find that the latter dominates the former.

■ ASSOCIATED CONTENT

Supporting Information

The Supporting Information is available free of charge on the ACS Publications website at DOI: 10.1021/jacs.8b05271.

Synthesis conditions of MOFs in this work and their structure refinement procedures (PDF)

X-ray crystallographic data (CIF files) for MOF-1004, UiO-66, and UiO-67 structures (ZIP)

■ AUTHOR INFORMATION

Corresponding Author

*yaghi@berkeley.edu

ORCID

Omar M. Yaghi: 0000-0002-5611-3325

Notes

The authors declare no competing financial interest.

■ ACKNOWLEDGMENTS

Support for the synthesis and the characterization of compounds was provided by King Abdulaziz City for Science and Technology (Center of Excellence for Nanomaterials and Clean Energy Applications). We thank Dr. Simon J. Teat and Dr. Laura J. McCormick for the synchrotron X-ray diffraction data acquisition support at the beamlines 11.3.1 and later 12.2.1 (Advanced Light Source, Lawrence Berkeley National Laboratory). We thank Christian S. Diercks for editing the manuscript. This research used resources of the Advanced Light Source, which is a DOE Office of Science User Facility under contract no. DE-AC02-05CH11231.

■ REFERENCES

(1) Debye, P. *Ann. Phys.* **1913**, *348*, 49−92.

(2) Waller, I. *Eur. Phys. J. A* **1923**, *17*, 398−408.

(3) Furukawa, H.; Cordova, K. E.; O'Keeffe, M.; Yaghi, O. M. *Science* **2013**, *341*, 1230444.

(4) Chae, H. K.; Siberio-Pérez, D. Y.; Kim, J.; Go, Y.; Eddaoudi, M.; Matzger, A. J.; O'Keeffe, M.; Yaghi, O. M. *Nature* **2004**, *427*, 523.

(5) Cavka, J. H.; Jakobsen, S.; Olsbye, U.; Guillou, N.; Lamberti, C.; Bordiga, S.; Lillerud, K. P. *J. Am. Chem. Soc.* **2008**, *130*, 13850−13851.

(6) Valenzano, L.; Civalleri, B.; Chavan, S.; Bordiga, S.; Nilsen, M. H.; Jakobsen, S.; Lillerud, K. P.; Lamberti, C. *Chem. Mater.* **2011**, *23*, 1700−1718.

(7) Kitagawa, S.; Kitaura, R.; Noro, S. *Angew. Chem., Int. Ed.* **2004**, *43*, 2334−2375.

(8) Ranocchiari, M.; van Bokhoven, J. A. *Chimia* **2013**, *67*, 397−402.

(9) Zhang, J.-P.; Liao, P.-Q.; Zhou, H.-L.; Lin, R.-B.; Chen, X.-M. *Chem. Soc. Rev.* **2014**, *43*, 5789−5814.

(10) Schneemann, A.; Bon, V.; Schwedler, I.; Senkovska, I.; Kaskel, S.; Fischer, R. A. *Chem. Soc. Rev.* **2014**, *43*, 6062−96.

(11) Kim, Y.; Haldar, R.; Kim, H.; Koo, J.; Kim, K. *Dalton Trans.* **2016**, *45*, 4187−4192.

DOI: 10.1021/jacs.8b05271
J. Am. Chem. Soc. 2018, 140, 8958−8964

(12) Bennett, T. D.; Fuchs, A. H.; Cheetham, A. K.; Coudert, F.-X. *Dalton Trans.* **2016**, *45*, 4058−4059.
(13) Brozek, C. K.; Michaelis, V. K.; Ong, T.-C.; Bellarosa, L.; López, N.; Griffin, R. G.; Dincă, M. *ACS Cent. Sci.* **2015**, *1*, 252−260.
(14) Yeung, H. H.-M.; Wu, Y.; Henke, S.; Cheetham, A. K.; O'Hare, D.; Walton, R. I. *Angew. Chem., Int. Ed.* **2016**, *55*, 2012−2016.
(15) Wilson, A. J. C. *Nature* **1942**, *150*, 152.
(16) Dunitz, J. D.; Schomaker, V.; Trueblood, K. N. *J. Phys. Chem.* **1988**, *92*, 856−867.
(17) O'Keeffe, M.; Peskov, M. A.; Ramsden, S. J.; Yaghi, O. M. *Acc. Chem. Res.* **2008**, *41*, 1782−1789.
(18) Wang, B.; Lv, X.-L.; Feng, D.; Xie, L.-H.; Zhang, J.; Li, M.; Xie, Y.; Li, J.-R.; Zhou, H.-C. *J. Am. Chem. Soc.* **2016**, *138*, 6204−6216.
(19) Delgado-Friedrichs, O.; O'Keeffe, M.; Yaghi, O. M. *Phys. Chem. Chem. Phys.* **2007**, *9*, 1035−1043.
(20) Karplus, P. A.; Diederichs, K. *Science* **2012**, *336*, 1030−1033.
(21) Inokuma, Y.; Yoshioka, S.; Ariyoshi, J.; Arai, T.; Hitora, Y.; Takada, K.; Matsunaga, S.; Rissanen, K.; Fujita, M. *Nature* **2013**, *495*, 461.
(22) Lee, S.; Kapustin, E. A.; Yaghi, O. M. *Science* **2016**, *353*, 808−811.
(23) Borrmann, H.; Persson, I.; Sandström, M.; Stålhandske, C. M. V. *J. Chem. Soc., Perkin Trans. 2* **2000**, *0*, 393−402.
(24) Nishida, J.; Tamimi, A.; Fei, H.; Pullen, S.; Ott, S.; Cohen, S. M.; Fayer, M. D. *Proc. Natl. Acad. Sci. U. S. A.* **2014**, *111*, 18442−18447.

DOI: 10.1021/jacs.8b05271
J. Am. Chem. Soc. 2018, 140, 8958−8964